COMMUNICATION

Advancing Pore-Space-Partitioned Metal-Organic Frameworks with Isoreticular Cluster Concept

Yuchen Xiao,[a] Yichong Chen, [a] Wei Wang,[a] Xianhui Bu,*[b] and Pingyun Feng*[a]

[a] Dr. Y. Xiao, Y. Chen, Dr. W. Wang, Prof. P. Feng
Department of Chemistry
University of California, Riverside
900 University Ave, Riverside, CA 92521 (USA)
E-mail: pingyun.feng@ucr.edu

[b] Prof. X. Bu
Department of Chemistry and Biochemistry
California State University Long Beach
1250 Bellflower Boulevard, Long Beach, CA 90840 (USA)
E-mail: xianhui.bu@csulb.edu

Supporting information for this article is given via a link at the end of the document.

Abstract: Trigonal planar M_3(O/OH) trimers are among the most important clusters in inorganic chemistry and are the foundational features of multiple high-impact MOF platforms. Here we introduce a concept called isoreticular cluster series and demonstrate that M_3(O/OH), as the first member of a supertrimer series, can be combined with a higher hierarchical member (double-deck trimer here) to advance isoreticular chemistry. We report here an isoreticular series of pore-space-partitioned MOFs called M_3M_6 *pacs* made from co-assembly between M_3 single-deck trimer and M_{3x2} double-deck trimer. Important factors were identified on this multi-modular MOF platform to guide optimization of each module, which enables the phase selection of M_3M_6 *pacs* by overcoming the formation of previously-always-observed same-cluster phases. The new *pacs* materials exhibit high surface area and high uptake capacity for CO_2 and small hydrocarbons, as well as selective adsorption properties relevant to separation of industrially important mixtures such as C_2H_2/CO_2 and C_2H_2/C_2H_4. Furthermore, new M_3M_6 *pacs* materials show electrocatalytic properties with high activity.

In the pre-crystallization mixture for solvothermal synthesis of open-framework materials ranging from metal chalcogenides to metal-organic frameworks (MOFs), inorganic clusters of different types and sizes could co-exist, opening up opportunities for selecting various crystallization pathways via different combinations of clusters.[1] Of great significance in materials design is the understanding of chemical and structural factors that contribute to the formation and selection of specific cluster types in the crystallized products.[2] A special challenge is the ability to stabilize different cluster types and to enable their co-assembly. Such heterogenization of framework building blocks is useful for diversifying framework materials to tune their properties.

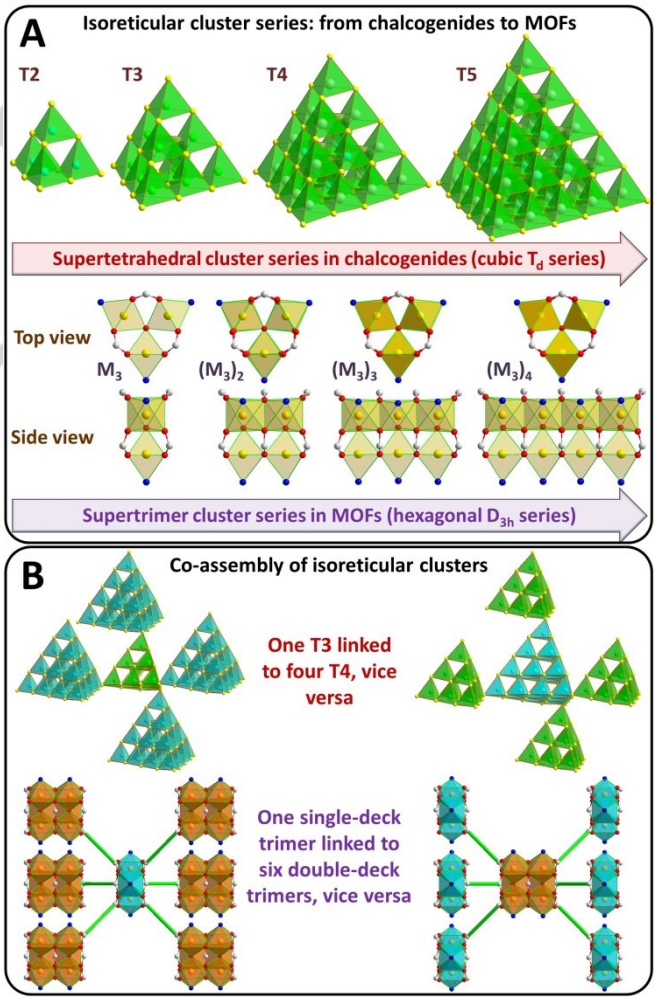

Scheme 1. (A) Two types of isoreticular cluster series.[3] Among them, $(M_3)_3$ and $(M_3)_4$ remain to be developed. (B) The co-assembly of different isoreticular clusters in UCR-19 chalcogenide and M_3M_6-bco *pacs* (this work).

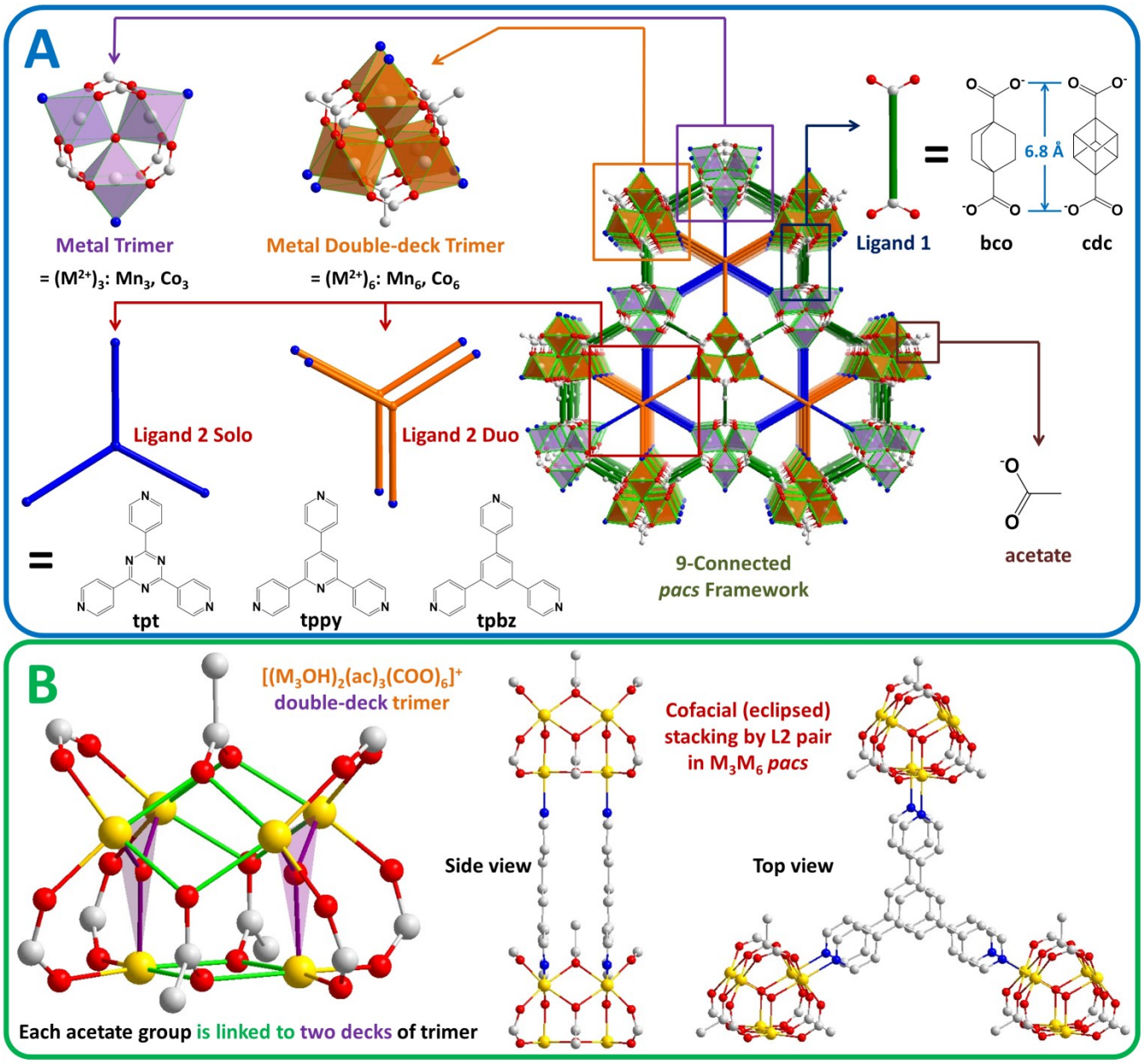

Figure 1. (A) Illustration of the M_3M_6 *pacs* system. bco = bicyclo[2.2.2]octane-1,4-dicarboxylate, cdc = 1,4-cubanedicarboxylate, tpt = 2,4,6-tri(4-pyridyl)-1,3,5-triazine, tppy = 2,4,6-tris(4-pyridyl)pyridine, tpbz = 1,3,5-tri(4-pyridyl)benzene. (B) Structure of $[(M_3OH)_2(ac)_3(COO)_6]^+$ double-deck trimer and cofacial stacking by L2 pair in M_3M_6-bco *pacs*.

We have long been interested in heterogenizing framework building units to tune materials' properties. Our approach has relied on using charge-complementary metal ions (e.g., M^{2+}/M^{3+} in phosphate zeotypes, M^{3+}/M^{4+} in chalcogenide zeotypes, M^{2+}/M^{3+} in trimer-MOFs).[3a, 4] Only in chalcogenides, were we able to achieve isoreticular chemistry with clusters of different sizes (e.g., supertetrahedral $Ga_{10}S_{18}^{6-}$ T3 and $Zn_4Ga_{16}S_{33}^{10-}$ T4 clusters in UCR-19, **Scheme 1**).[3b] Prior to this work, we have no success in making MOFs from different-sized isoreticular clusters. In fact, while isoreticular chemistry is easy with different metal ions or ligands, rarely does it involve clusters of different sizes. The concept of isoreticular clusters (isoclusters) is similar to the recently introduced bioisosteric (BIS) concepts for organic ligands,[4e, 5] since both address strategies for developing isoreticular building blocks with comparable bond vectors (but different core) needed in isoreticular-chemistry-based MOF discovery.[6]

One limitation in realizing cluster-size heterogenization is likely from the simple composition of many MOF platforms consisting of just one metal type and one crosslinking-ligand type. Such compositions offer fewer opportunities to introduce complementary features often needed to establish more complex chemical systems or drive more complex processes. We have therefore focused more on multi-modular MOF platforms. The

past decade has seen the growth of a family of isoreticular pore-space-partitioned (PSP) MOFs called *pacs* (*pacs* = partitioned *acs*), a multi-modular system formulated as $[M_3(O/OH)(L1)_3(L2)]$ (called **M_3 *pacs*** here), where L1 (ligand 1) is used for forming the *acs* net (MIL-88/MOF-235) and L2 (ligand 2) is a pore-partitioning ligand.[4c-e, 5, 7] Interestingly, three *pacs* materials containing Mn_6 clusters (NPU-1/2/3) were recently reported.[8] These past studies on the same-cluster M_3- or M_6-*pacs* materials raised the prospect for the co-existence of isoreticular clusters, similar to the co-existence of supertetrahedral chalcogenide clusters (**Scheme 1**).

Here, we report a new category of *pacs* materials with the distinction of being the first to be crystallized from the co-assembly of the first two members of an isoreticular supertrimer series (i.e., single-deck M_3 trimer and M_{3x2} double-deck trimer, **Scheme 1**) as shown by the formula $[[M_3(OH)][(M_3OH)_2(ac)_3](L1)_6(L2)_3]$ (called **M_3M_6 *pacs***, **Figure 1A**). By overcoming the previously-always-observed tendency to form same-cluster *pacs*, the formation of the mixed-cluster *pacs* reported here is unusual and compels us to study various modules and related factors from a different perspective. We found that the mixed-cluster *pacs* materials result from the convergence and balance of multiple chemical and structural features (**Figure S8.5**). These new M_3M_6 *pacs* materials have high surface area and high uptake capacity for common gases, together with selective sorptive properties relevant to separation of important mixtures such as C_2H_2/CO_2 and C_2H_2/C_2H_4. Also, they show electrocatalytic properties with high activity.

The M_3M_6 *pacs* can be made as either Mn- or Co-*pacs* with **bco** or **cdc** as L1 ligand (**Figure 1A**) in the non-centrosymmetric space group *P*-6*m*2. The pore-partition ligands (L2) identified to form M_3M_6 *pacs* are **tpt**, **tppy**, **tpbz** (**Figure 1A**). Among twelve possible M_3M_6 *pacs* from these M-L1-L2 combinations, eleven have been made (Mn_3Mn_6-bco-tpt not yet synthesized, **Table S2**). For comparative studies, also reported here are one new M_6 pacs (Mn_6-bdc-tpbz) and 23 new M_3 *pacs* (M = Mg^{2+}, Mn^{2+}, Co^{2+}, Ni^{2+}, L1 = benzene-1,4-dicarboxylate (**bdc**), bicyclo[1.1.1]pentane-1,3-dicarboxylate (**bcp**), cdc, bco; L2 = tpt, tppy, tpbz) (**Table S2**).[9]

The M_3M_6 *pacs* offers a new way to control charge of the building block and framework. M_3M_6 *pacs* consists of two isoreticular clusters, $[M_3(OH)(COO)_6]^-$ trimer (**Figure S2.3**) and $[(M_3OH)_2(ac)_3(COO)_6]^+$ double-deck trimer (**Figure 1B** and **Figures S2.4-S2.5**). The double-deck trimer is formed by linking two single-deck trimers with three acetate ligands. Since M_3 and M_6 have the same D_{3h} symmetry and are both 9-connected, the substitution of M_3 with M_6 still conforms to the site symmetry of the inorganic nodes, which is why isoreticular chemistry is preserved. For M^{2+}, a single-deck trimer carries -1 charge and the resulting same-cluster M_3 *pacs* framework would be anionic. With each extra deck, a $[M_3(OH)(ac)_3]^{2+}$ unit is added, leading to an increase of +2 in the charge so that the double-deck trimer carries +1 charge (**Figure S3.5**). Thus, the 1:1 mixing between single- and double-deck trimers gives a neutral framework (**Figure S10.1**). In M_3M_6 *pacs*, through L1 ligand, each M_3 trimer is linked to 6 double-deck trimers (**Figures S2.7A**, **S2.8**), and vice versa (**Figures S2.7B**, **S2.9**). The M_3M_6 framework can be visualized as alternating negative M_3 and positive M_6 layers along the *c* axis in staggered configuration.

Our comparative studies show that the structural property of L1 ligand is a contributing factor to the occurrence of M_6 double-deck trimer. To help explain the M_6 formation, we turned our attention to the possible L1-L1 steric repulsion between three L1 ligands above the trimer plane and three L1 ligands below the trimer plane (**Figure S5.3**), such steric repulsion would increase if L1 ligands are bulkier, but should be reduced by the M_6 formation. Therefore, we can suggest that bulkier L1 would increase the probability for forming M_3M_6 *pacs*.

We selected four L1 ligands (H_2bdc, H_2bcp, H_2cdc, H_2bco) to compare their effects (**Figure 2** and **Figure S8.1**). Not surprisingly, the planar 2-D ligand bdc (C_6H_4 core) did not produce M_6, leading to the same-cluster M_3 *pacs*. For bcp, cdc, and bco, they all have a 3-D core. Based on the number of core carbon and hydrogen atoms, the degree of their bulkiness can be ranked as bcp (C_5H_6) < cdc (C_8H_6) < bco (C_8H_{12}). Experimentally, we found that bcp also gives M_3 *pacs*. Apparently, for small bcp ligand, L1-L1 interactions are insignificant. For cdc and bco ligands with bulky and protruding cores, L1-L1 interactions may be significant enough so that M_3 and M_6 clusters can co-exist in the reaction mixtures. (**Figure S5.3**). Whether bco and cdc forms M_3 *pacs* or M_3M_6 *pacs* also depends on other factors.

The next factor that can move the equilibrium between M_3 *pacs* and M_3M_6 *pacs* is the nature of pore-partition ligands (L2). Past studies have shown that M_3 *pacs* can accommodate a wide range of L2 types. However, here we found that the formation of M_3M_6 *pacs* is sensitive to L2 type. This is due to a prominent difference between M_3 *pacs* and M_3M_6 *pacs* in terms of ligand-ligand interaction (L2 to L2) which is absent in M_3 *pacs*, but is an unavoidable feature in M_3M_6 *pacs*. Because of the co-existence of single- and double-deck trimers in M_3M_6 *pacs*, there are two accompanying L2 arrangements: single-deck L2 and double-deck L2. Constrained by coordination with double-deck trimers, the L2 pair has no choice but to adopt an unusual cofacial pi-stacked configuration between four 6-membered aromatic rings (**Figure 1B** and **Figure S2.12**).[10] The separation between L2 pair is related to the gap between two trimer decks. Of great influence on the competing formation of M_3 *pacs* and M_3M_6 *pacs* is the fact that the gap between trimer decks (related to ionic radii of M^{2+}), is around 338-352 pm (M-M distance, for M_3M_6-bco *pacs*, **Figure S5.5**) which is close to the minimum pi-pi stacking separation (about 340 pm, based on van der Waals radius of 170 pm for C). As a result, chemical properties of L2 ligands that can help or hinder the formation of the L2 pair play a key role in the phase selection between M_3 *pacs* and M_3M_6 *pacs*.

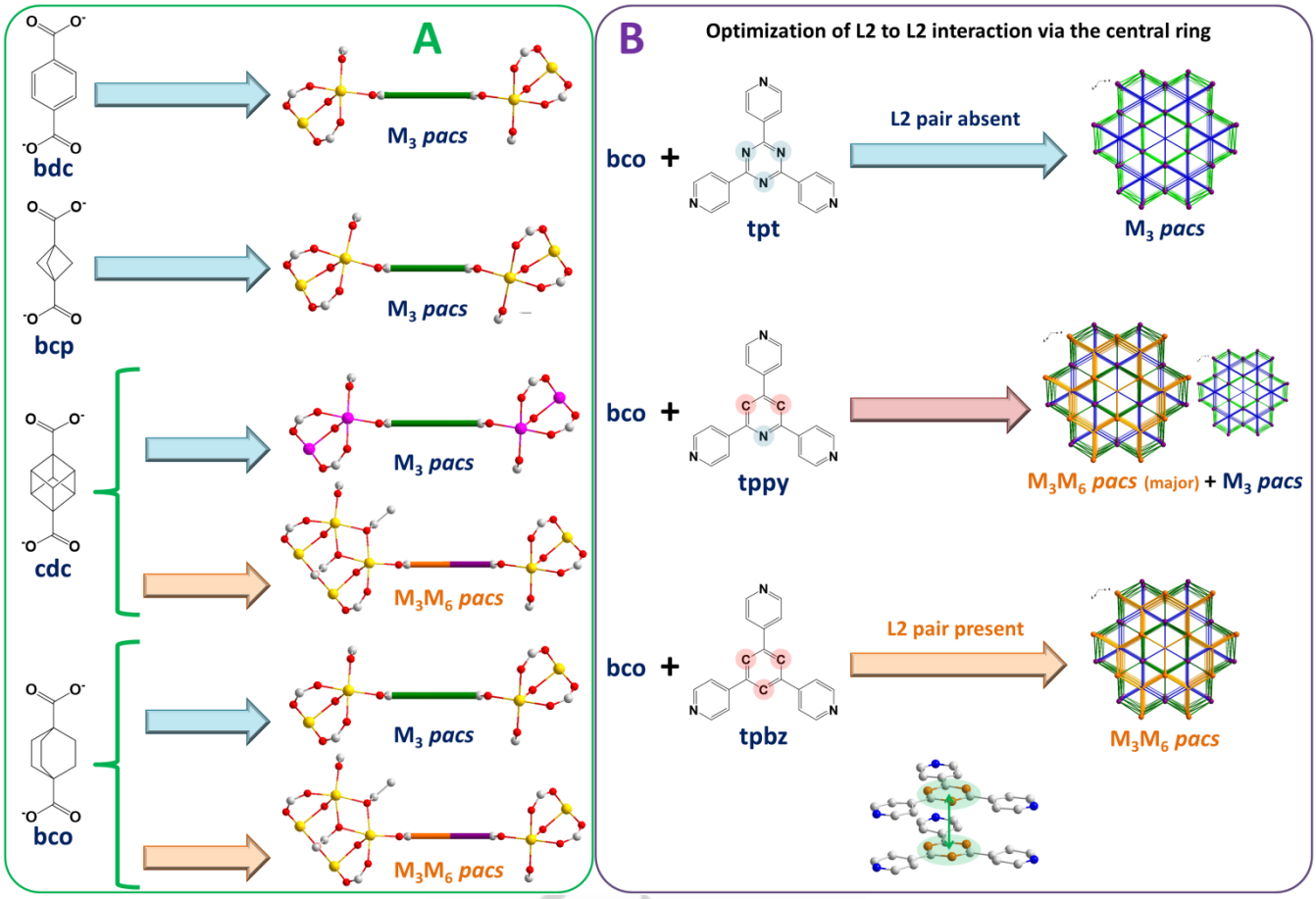

Figure 2. Sequentially optimized synthesis of M_3M_6 *pacs* by tuning ligand 1 (A) and fine-tuning ligand 2 (B). The illustrated phase selectivity in (B) is for Mn-*pacs*.

We studied five different L2 ligands with L1 bco. They are N,N-di-4-pyridinyl-4-pyridinamine (**tpa**), tpt, tppy, tpbz, and 2,5,8-tri-(4-pyridyl)-1,3,4,6,7,9-hexaazaphenalene) (**H-tph**) (**Figures S1.4**, **S8.2**). Neither tpa nor tph have been found to form M_3M_6 *pacs*. For tpa, there is only one nitrogen atom at the core, the cofacial stacking of two electronegative N atoms (plus 3 pyridine rings) seems less probable. Likewise, tph tends to carry a negative charge at its core which can hinder the formation of L2 pair. Note that tpa and tph can easily form M_3 *pacs* because observed L2-L2 separation is > 500 pm in M_3 *pacs* so that no L2-L2 interactions are present.[7g, 11]

For tpt, tppy, and tpbz, which have a 6-membered aromatic ring at the core (**Figure 1A**), their phase-selection behavior for M_3 *pacs* and M_3M_6 *pacs* is subtly different. These L2 ligands allow the fine-tuning of L2-L2 interaction for better synergy with attached double-deck trimers. We found that the ability to form M_3M_6 *pacs* over M_3 *pacs* follows the order tpbz > tppy > tpt. This is based on our synthesis results that for Mn-bco-*pacs*, tpbz gives M_3M_6 *pacs*, tppy gives both M_3M_6 *pacs* and M_3 *pacs*, and tpt gives M_3 *pacs* (**Figure 2**). Additionally, for Co-bco-*pacs*, both tpbz and tppy give M_3M_6 *pacs*, while tpt gives a mixture of M_3M_6 *pacs* and M_3 *pacs*. This trend is related to the cofacial (eclipsed) stacking by L2 pairs which can be more easily achieved by benzene rings than by pyridine/triazine rings with one/three electronegative N atoms that should be less favorable in the eclipsed configuration.

By using optimized L1 ligand (bco) and L2 ligand (tpbz > tppy > tpt), we studied the phase selectivity by metal ions such as Mn^{2+}, Co^{2+}, Ni^{2+}, and Zn^{2+} (**Figure S8.2**). So far, only Mn^{2+} and Co^{2+} have formed M_3M_6 *pacs*. Various factors such as ionic radii and electron configuration could play a role. Our analysis indicates that compared to M_3 *pacs* that can take metal ions with a large range of ionic radii from 62 pm (Cr^{3+}) to 95 pm (Cd^{2+}),[7f, 7h, 12] the range of ionic radii for M_3M_6 *pacs* is narrower to better accommodate the formation of double-deck trimers and cofacially stacked L2 pairs (**Figure S5.5**). We note that a decrease in ionic radii of metal ions (e.g., from Mn^{2+} 83 pm high spin to Co^{2+} 74.5 pm high spin) would cause an overall shrinkage of double-deck trimers (i.e., shorter M to M distance within M_6 cluster, 11-13 pm decrease from Mn-bco to Co-bco, **Figure S5.5**) which could have significant consequence on the formation of M_6 clusters and L2 pairs.[12a] There is a limit to how small the metal ions could be since the L2-L2 distance (358-364 pm) and acetate-acetate distance (280-286 pm between adjacent O sites) in Mn_3Mn_6-bco *pacs* and Co_3Co_6-bco *pacs* are already short enough compared to the sum of van der Waals radii (**Figure S5.7**). Any factor (e.g., smaller metal ions) that requires L2 pairs and acetate-acetate-

acetate triangles to contract further may cause unfavorable repulsion and prevent the formation of M_3M_6 *pacs*. So far, M_3M_6 *pacs* has not yet been made from Ni^{2+} (69 pm), likely due to the extra difficulty from its smaller size compared to Mn^{2+} and Co^{2+}.[12a] For Zn^{2+} (74 pm),[12a] its d^{10} configuration make it more accommodative of different coordination numbers (4-6), leading to more pre-nucleation species and crystallization pathways and reduced probability to competitively form M_3M_6 *pacs*.

The above discussions suggest that L1-L1 interaction, L2-L2 interaction, and the type of metal ions all have impact on the formation of M_3M_6 *pacs*. While L1-L1 repulsion helps the formation of M_6, L2-L2 interaction has the opposite effect. The strength of L1-L1 and L2-L2 interactions is affected by both structures of ligands and properties of metal ions. Given the complexity of the multi-modular co-assembly, other synthetic parameters and structural features (e.g., pH, acetate concentration) could impact the equilibrium between M_3 and M_6 clusters and products as shown by the synthesis of NPU-1/2/3 M_6-pacs from planar aromatic ligands. The discussions here are based on keeping other synthetic conditions as identical as possible. Ligand-ligand interactions have been shown by Yaghi et al. to affect the framework topology in ZIFs.[13] Here in the multi-module *pacs* system, there are two different ligand-ligand interactions in competition. Instead of affecting the framework topology, they impact the type of clusters in the final products.

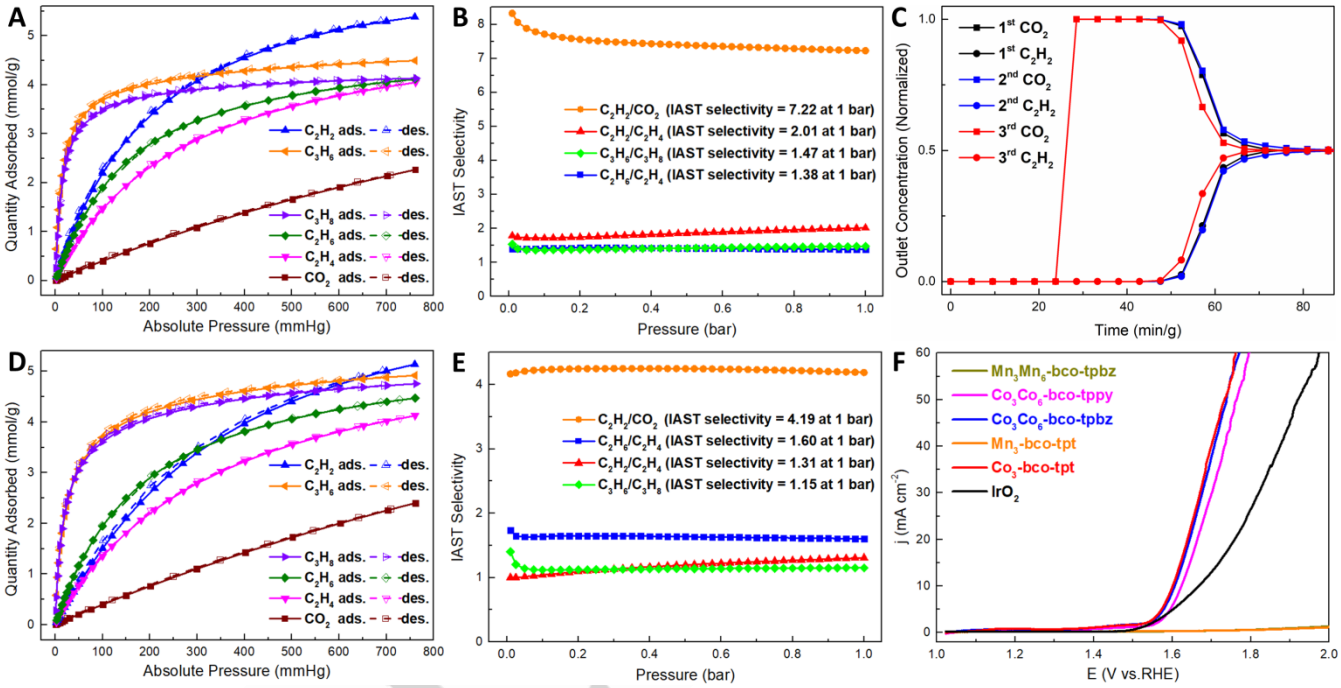

Figure 3. Gas adsorption isotherms of Co_3Co_6-bco-tppy (A) and Co_3-bco-tpt at 298 K (D). The IAST (50/50 v/v) selectivities for various gas pairs at 298 K of Co_3Co_6-bco-tppy (B) and Co_3-bco-tpt (E). Three cycles of experimental breakthrough curves at room temperature with an equimolar C_2H_2/CO_2 gas mixtures for Co_3Co_6-bco-tppy (C). For OER, the LSV curves of different catalysts (F).

Thermal stability of M_3M_6-bco *pacs* (**Figures S6.1-S6.2**) and M_3-bco *pacs* (**Figures S6.5-S6.7**) were studied by TGA and all samples remained stable up to about 300 °C. Different compositions of M_3M_6-bco *pacs* and M_3-bco *pacs* were used for gas sorption studies. PXRD shows no difference in diffraction patterns before and after sorption, suggesting all samples were stable after adsorption test (**Figures S6.1-S6.2** and **Figures S6.6-S6.7**). The Brunauer–Emmett–Teller (BET) surface area from N_2 sorption at 77 K (**Figure S9.1**) ranges from 921 to 1048 m^2/g for M_3M_6-bco *pacs* and from 951 to 1020 m^2/g for M_3-bco *pacs* (**Table S4.2**), indicative of high porosity.

M_3M_6-bco *pacs* has enhanced C_2H_2/CO_2 selective adsorption property over M_3-bco *pacs*. At 298 K and 1 atm, the C_2H_2 and CO_2 uptakes are 5.12 and 2.01 mmol/g for Mn_3Mn_6-bco-tpbz, 5.38 and 2.27 mmol/g for Co_3Co_6-bco-tppy, and 5.12 and 2.11 mmol/g for Co_3Co_6-bco-tpbz (**Figure 3A** and **Figures S9.2-S9.4**, **Table S4.2**). In comparison, for M_3-bco *pacs* at 298 K and 1 atm, the C_2H_2 and CO_2 uptake are 4.77 and 2.13 mmol/g for Mn_3-bco-tpt, and 5.14 and 2.40 mmol/g for Co_3-bco-tpt (**Figure 3D** and **Figures S9.5-S9.6**, **Table S4.2**). The isotherms of C_2H_2 and CO_2 at 298 K were used to fit with the Dual-Site Langmuir-Freundlich (DSLF) model to calculate the ideal adsorbed solution theory (IAST, 50/50) selectivities. M_3M_6 *pacs* including Mn_3Mn_6-bco-tpbz (6.23), Co_3Co_6-bco-tppy (7.22), and Co_3Co_6-bco-tpbz (6.80) show better C_2H_2/CO_2 selective adsorption property than M_3 *pacs* such as Mn_3-bco-tpt (4.45), and Co_3-bco-tpt (4.19). (**Figures 3B**, **3E** and **Figures S9.2-S9.6**, **Table S4.5**). The breakthrough experiments showed that Co_3Co_6-bco-tppy has a long breakthrough time and excellent separation performance for C_2H_2/CO_2 (**Figure 3C**).

We also explored the selective adsorption capacity for C2 gases of M_3M_6-bco *pacs*, because the C_2H_4 purification directly from $C_2H_2/C_2H_4/C_2H_6$ three-component mixture is of great significance.[8, 14] At 298 K and 1 atm, for Co_3Co_6-bco-tppy, the C_2H_2, C_2H_4, and C_2H_6 uptakes are 5.38, 4.05 and 4.12 mmol/g, respectively (**Figure 3A** and **Figure S9.3**, **Table S4.2**). In comparison, for Co_3-bco-tpt at 298 K and 1 atm, the C_2H_2, C_2H_4, and C_2H_6 uptake are 5.14, 4.13 and 4.47 mmol/g, respectively (**Figure 3D** and **Figure S9.6**, **Table S4.2**). The isotherms of C_2H_2, C_2H_4, and C_2H_6 at 298 K were used to fit with the DSLF model to calculate the IAST (50/50) selectivities. For Co_3Co_6-bco-tppy, the selectivity is 2.01 (C_2H_2/C_2H_4) and 1.38 (C_2H_6/C_2H_4) (**Figure 3B**, **Table S4.5**), and for Co_3-bco-tpt, the selectivity is 1.31 (C_2H_2/C_2H_4) and 1.60 (C_2H_6/C_2H_4) (**Figure 3E**, **Table S4.5**). Other M_3M_6-bco *pacs* and M_3-bco *pacs* show similar properties for $C_2H_2/C_2H_4/C_2H_6$ (**Figures S9.2**, **S9.4**, **S9.5**, **Table S4.5**). M_3M_6-bco *pacs* has better C_2H_2/C_2H_4 selective adsorption property than M_3-bco *pacs*, but M_3-bco *pacs* has higher C_2H_6/C_2H_4 inverse selectivity than M_3M_6-bco *pacs*. In addition, M_3M_6-bco *pacs* has benzene/cyclohexane selective adsorption property (**Figures S11.1-S11.4**, **Table S5.2**).

Co_3Co_6-bco *pacs* has good electrocatalytic activity for oxygen evolution reaction (**OER**). Linear sweep voltammetry (LSV) curves of different samples are investigated (**Figure 3F**). Both Co_3Co_6-bco-tppy and Co_3Co_6-bco-tpbz have relatively low overpotential of 376-393 mV at current density of 10 mA cm^{-2} and low Tafel slope of 87.1-95.1 mV dec^{-1}, which is better than IrO_2 (**Figure S12.1**).

In conclusion, a series of highly porous pore-space-partitioned metal-organic frameworks have been synthesized from the co-assembly between isoreticular M_3 single-deck trimer and M_{3x2} double-deck trimer. The formation of M_3M_6 *pacs* results from the synergistic co-assembly of multiple structural components including M_3 cluster, M_6 cluster, L1, solo L2, and L2-L2 pair. The work reported here reveals greater scope of isoreticular chemistry enabled by isoreticular cluster concept. Further challenges and opportunities could come from the expansion of new isoreticular clusters and applications of isoreticular clusters to MOF platforms beyond the *pacs* platform reported here.

Supporting Information

The authors have cited additional references within the Supporting Information.[15]

Acknowledgements

We acknowledge the support of this work by the US Department of Energy, Office of Basic Energy Sciences, Materials Sciences and Engineering Division under Award No. DE-SC0010596 (P.F.). The electrocatalytic studies of the synthesized materials were supported by the National Science Foundation (CHEM 2154375, P. F.). Single-crystal X-ray diffraction studies made use of an instrument obtained with an NSF MRI grant (CHEM 2117040, X. B.).

Keywords: Isoreticular cluster • porosity • gas separation • adsorption • electrocatalysis

[1] a) X. Bu, N. Zheng, P. Feng, *Chem. Eur. J.* **2004**, *10*, 3356-3362; b) P. Feng, X. Bu, N. Zheng, *Acc. Chem. Res.* **2005**, *38*, 293-303; c) J. Zhang, X. Bu, P. Feng, T. Wu, *Acc. Chem. Res.* **2020**, *53*, 2261-2272; d) S.-T. Zheng, T. Wu, C. Chou, A. Fuhr, P. Feng, X. Bu, *J. Am. Chem. Soc.* **2012**, *134*, 4517-4520; e) S.-T. Zheng, J. J. Bu, T. Wu, C. Chou, P. Feng, X. Bu, *Angew. Chem. Int. Ed.* **2011**, *50*, 8858-8862.

[2] a) S. Mitzinger, L. Broeckaert, W. Massa, F. Weigend, S. Dehnen, *Nat. Commun.* **2016**, *7*, 10480; b) B. Weinert, S. Mitzinger, S. Dehnen, *Chem. Eur. J.* **2018**, *24*, 8470-8490.

[3] a) N. Zheng, X. Bu, B. Wang, P. Feng, *Science* **2002**, *298*, 2366-2369; b) N. Zheng, X. Bu, P. Feng, *J. Am. Chem. Soc.* **2003**, *125*, 1138-1139; c) X. Bu, N. Zheng, Y. Li, P. Feng, *J. Am. Chem. Soc.* **2003**, *125*, 6024-6025; d) X. Bu, N. Zheng, Y. Li, P. Feng, *J. Am. Chem. Soc.* **2002**, *124*, 12646-12647.

[4] a) X. Bu, P. Feng, G. D. Stucky, *Science* **1997**, *278*, 2080-2085; b) P. Feng, X. Bu, G. D. Stucky, *Nature* **1997**, *388*, 735-741; c) H. Yang, Y. Wang, R. Krishna, X. Jia, Y. Wang, A. N. Hong, C. Dang, H. E. Castillo, X. Bu, P. Feng, *J. Am. Chem. Soc.* **2020**, *142*, 2222-2227; d) Y. Xiao, A. N. Hong, Y. Chen, H. Yang, Y. Wang, X. Bu, P. Feng, *Small* **2023**, *19*, 2205119; e) Y. Xiao, Y. Chen, W. Wang, H. Yang, A. N. Hong, X. Bu, P. Feng, *J. Am. Chem. Soc.* **2023**, *145*, 10980-10986.

[5] a) H. Yang, Y. Chen, C. Dang, A. N. Hong, P. Feng, X. Bu, *J. Am. Chem. Soc.* **2022**, *144*, 20221-20226; b) W. Wang, H. Yang, Y. Chen, X. Bu, P. Feng, *J. Am. Chem. Soc.* **2023**, *145*, 17551-17556; c) Y. Chen, H. Yang, W. Wang, X. Li, Y. Wang, A. N. Hong, X. Bu, P. Feng, *Small* **2023**, *19*, 2303540.

[6] a) M. Eddaoudi, J. Kim, N. Rosi, D. Vodak, J. Wachter, M. O'Keeffe, O. M. Yaghi, *Science* **2002**, *295*, 469-472; b) H. Cui, Y. Ye, T. Liu, Z. A. Alothman, O. Alduhaish, R.-B. Lin, B. Chen, *Inorg. Chem.* **2020**, *59*, 17143-17148; c) A. Dutta, Y. Pan, J.-Q. Liu, A. Kumar, *Coord. Chem. Rev.* **2021**, *445*, 214074; d) R.-B. Lin, Z. Zhang, B. Chen, *Acc. Chem. Res.* **2021**, *54*, 3362-3376.

[7] a) X. Zhao, X. Bu, Q.-G. Zhai, H. Tran, P. Feng, *J. Am. Chem. Soc.* **2015**, *137*, 1396-1399; b) Q.-G. Zhai, X. Bu, C. Mao, X. Zhao, L. Daemen, Y. Cheng, A. J. Ramirez-Cuesta, P. Feng, *Nat. Commun.* **2016**, *7*, 13645; c) X. Zhao, X. Bu, E. T. Nguyen, Q.-G. Zhai, C. Mao, P. Feng, *J. Am. Chem. Soc.* **2016**, *138*, 15102-15105; d) Y. Wang, X. Zhao, H. Yang, X. Bu, Y. Wang, X. Jia, J. Li, P. Feng, *Angew. Chem. Int. Ed.* **2019**, *58*, 6316-6320; e) A. N. Hong, H. Yang, T. Li, Y. Wang, Y. Wang, X. Jia, A. Zhou, E. Kusumoputro, J. Li, X. Bu, P. Feng, *ACS Appl. Mater. Interfaces* **2021**, *13*, 52160-52166; f) H. Yang, F. Peng, A. N. Hong, Y. Wang, X. Bu, P. Feng, *J. Am. Chem. Soc.* **2021**, *143*, 14470-14474; g) A. N. Hong, E. Kusumoputro, Y. Wang, H. Yang, Y. Chen, X. Bu, P. Feng, *Angew. Chem. Int. Ed.* **2022**, *61*, e202116064; h) Y. Xiao, Y. Chen, A. N. Hong, X. Bu, P. Feng, *Angew. Chem. Int. Ed.* **2023**, *62*, e202300721; i) A. N. Hong, Y. Wang, Y. Chen, H. Yang, E. Kusumoputro, X. Bu, P. Feng, *Chem. Eur. J.* **2023**, *29*, e202203547.

[8] B. Zhu, J.-W. Cao, S. Mukherjee, T. Pham, T. Zhang, T. Wang, X. Jiang, K. A. Forrest, M. J. Zaworotko, K.-J. Chen, *J. Am. Chem. Soc.* **2021**, *143*, 1485-1492.

[9] Deposition Numbers 2302373 (for Mn_3Mn_6-bco-tppy), 2302374 (for Mn_3Mn_6-bco-tpbz), 2302376 (for Co_3Co_6-bco-tppy), 2302377 (for Co_3Co_6-bco-tpbz), 2303097 (for Mn_3-bco-tpt), 2303098 (for Co_3-bco-tpt (2)), 2308989 (for Mn_3-bco-tppy), 2310726 (for Co_3-bco-tpt (1)), 2312068 (for Mg_3-bco-tpt), 2312069 (for Mg_3-bco-tpbz), 2323360 (for Mn_3-bcp-tppy), 2323361 (for Mn_3-bdc-tpbz), 2323506 (for Mn_6-bdc-tpbz), 2341853 (for Co_3-cdc-tpbz (1)), 2342059 (for Co_3-cdc-tpt (1)), 2341993 (for Mn_3-cdc-1), 2343925 (for Mn_3Mn_6-cdc-tpbz), 2343926 (for Co_3-cdc-tpbz (2)), 2343944 (for Co_3-cdc-tpt (2)), 2344762 (for Mn_3Mn_6-cdc-tpt), 2344763 (for Mn_3Mn_6-cdc-tppy), and 2344764 (for Co_3-cdc-tppy) contain the supplementary crystallographic data for this paper. These data are provided free of charge by the joint Cambridge Crystallographic Data Centre and Fachinformationszentrum Karlsruhe Access Structures service.

[10] a) R. Thakuria, N. K. Nath, B. K. Saha, *Cryst. Growth Des.* **2019**, *19*, 523-528; b) K. Carter-Fenk, J. M. Herbert, *Chem. Sci.* **2020**, *11*, 6758-6765.

[11] X. Mu, Y. Xue, M. Hu, P. Zhang, Y. Wang, H. Li, S. Li, Q. Zhai, *Chin. Chem. Lett.* **2023**, *34*, 107296.

[12] a) R. D. Shannon, *Acta Crystallogr. A* **1976**, *32*, 751-767; b) H.-R. Yang, W.-Y. Chen, D.-M. Chen, Y.-P. Zheng, S.-M. Fang, *J. Solid State Chem.* **2020**, *291*, 121658; c) Y.-Y. Xue, X.-Y. Bai, J. Zhang, Y. Wang, S.-N. Li, Y.-C. Jiang, M.-C. Hu, Q.-G. Zhai, *Angew. Chem. Int. Ed.* **2021**, *60*, 10122-10128.

[13] H. Hayashi, A. P. Côté, H. Furukawa, M. O'Keeffe, O. M. Yaghi, *Nat. Mater.* **2007**, *6*, 501-506.

[14] a) Z. Xu, X. Xiong, J. Xiong, R. Krishna, L. Li, Y. Fan, F. Luo, B. Chen, *Nat. Commun.* **2020**, *11*, 3163; b) L. Fan, P. Zhou, X. Wang, L. Yue, L. Li, Y. He, *Inorg. Chem.* **2021**, *60*, 10819-10829; c) Z. Jiang, L. Fan, P. Zhou, T. Xu, S. Hu, J. Chen, D.-L. Chen, Y. He, *Inorg. Chem. Front.* **2021**, *8*, 1243-1252; d) Y. Wang, C. Hao, W. Fan, M. Fu, X. Wang, Z. Wang, L. Zhu, Y. Li, X. Lu, F. Dai, Z. Kang, R. Wang, W. Guo, S. Hu, D. Sun, *Angew. Chem. Int. Ed.* **2021**, *60*, 11350-11358; e) P. Zhang, Y. Zhong, Y.

Zhang, Z. Zhu, Y. Liu, Y. Su, J. Chen, S. Chen, Z. Zeng, H. Xing, S. Deng, J. Wang, *Sci. Adv.* **2022**, *8*, eabn9231; f) J. Liu, J. Miao, H. Wang, Y. Gai, J. Li, *AIChE J.* **2023**, *69*, e18021.

[15] a) A. L. Myers, J. M. Prausnitz, *AIChE J.* **1965**, *11*, 121-127; b) H. Li, M. Eddaoudi, M. O'Keeffe, O. M. Yaghi, *Nature* **1999**, *402*, 276-279; c) A. Spek, *J. Appl. Crystallogr.* **2003**, *36*, 7-13; d) S. Shimomura, S. Horike, R. Matsuda, S. Kitagawa, *J. Am. Chem. Soc.* **2007**, *129*, 10990-10991; e) K. Li, J. Lee, D. H. Olson, T. J. Emge, W. Bi, M. J. Eibling, J. Li, *ChemComm* **2008**, 6123-6125; f) O. V. Dolomanov, L. J. Bourhis, R. J. Gildea, J. A. K. Howard, H. Puschmann, *J. Appl. Crystallogr.* **2009**, *42*, 339-341; g) D. Wang, B. Liu, S. Yao, T. Wang, G. Li, Q. Huo, Y. Liu, *ChemComm* **2015**, *51*, 15287-15289; h) Y. Xiao, N. Sheng, Y. Chu, Y. Wang, Q. Wu, X. Liu, F. Deng, X. Meng, Z. Feng, *Microporous Mesoporous Mater.* **2017**, *237*, 201-209; i) H.-G. Hao, Y.-F. Zhao, D.-M. Chen, J.-M. Yu, K. Tan, S. Ma, Y. Chabal, Z.-M. Zhang, J.-M. Dou, Z.-H. Xiao, G. Day, H.-C. Zhou, T.-B. Lu, *Angew. Chem. Int. Ed.* **2018**, *57*, 16067-16071; j) Y. Xiao, A. N. Hong, D. Hu, Y. Wang, X. Bu, P. Feng, *Chem. Eur. J.* **2019**, *25*, 16358-16365; k) W. Fan, S. Yuan, W. Wang, L. Feng, X. Liu, X. Zhang, X. Wang, Z. Kang, F. Dai, D. Yuan, D. Sun, H.-C. Zhou, *J. Am. Chem. Soc.* **2020**, *142*, 8728-8737; l) D. Hu, X. Wang, X. Chen, Y. Wang, A. N. Hong, J. Zhong, X. Bu, P. Feng, T. Wu, *J. Mater. Chem. A* **2020**, *8*, 11255-11260; m) A. A. Sapianik, K. A. Kovalenko, D. G. Samsonenko, M. O. Barsukova, D. N. Dybtsev, V. P. Fedin, *ChemComm* **2020**, *56*, 8241-8244; n) P. Liu, Y. Wang, Y. Chen, J. Yang, X. Wang, L. Li, J. Li, *Sep. Purif. Technol.* **2021**, *276*, 119284; o) D. Kim, B. N. Truong, D. Jo, J. W. Yoon, S.-K. Lee, Y.-S. Bae, K. Ho Cho, U. H. Lee, *Chem. Eng. J.* **2023**, *470*, 143858; p) M. K. Sahoo, A. K. Samantara, J. N. Behera, *Inorg. Chem.* **2020**, *59*, 12252-12262; q) Q. Zha, F. Yuan, G. Qin, Y. Ni, *Inorg. Chem.* **2020**, *59*, 1295-1305; r) X. Cai, F. Peng, X. Luo, X. Ye, J. Zhou, X. Lang, M. Shi, *ChemSusChem* **2021**, *14*, 3163-3173.

Entry for the Table of Contents

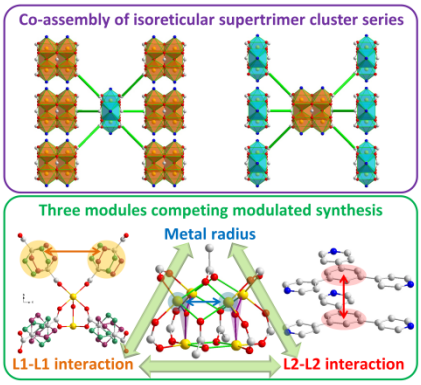

A new dimension to isoreticular chemistry is enabled by using isoreticular cluster concept to develop a series of hierarchical clusters whose co-assembly can follow different pathways dictated by a delicate balance between various competing chemical interactions.